

Effect of oxygen adsorption on the magnetoresistance of a disordered nanographite network

K. Takahara, K. Takai, and T. Enoki

Department of Chemistry, Tokyo Institute of Technology, 2-12-1 Ookayama, Meguro-ku, Tokyo 152-8551, Japan

K. Sugihara

1-40-6-506 Shibayama, Funabashi, Chiba 274-0816, Japan

(Received 21 August 2006; revised manuscript received 5 December 2006; published 30 July 2007)

Activated carbon fibers (ACFs), comprising a three-dimensional disordered network of metallic nanographite domains, have huge specific surface areas due to the presence of nanosized pores (nanopores) surrounded by nanographite domains. Around the edge of the nanographene sheets, there are localized spins originating from the nonbonding π -electron state (edge state). We investigate the effect of molecular adsorption on the magnetotransport of ACFs using oxygen, nitrogen, argon, and helium as the guest species. The magnetoresistance, which has a large positive value at the liquid helium temperature, is considerably reduced upon the adsorption of magnetic oxygen molecules in spite of the insensitivity to nonmagnetic molecular species. This change in the magnetoresistance induced by the oxygen molecule uptake can be explained in terms of the antiferromagnetic internal field of oxygen molecules affecting the edge-state spin. The change in the magnetoresistance yields the strength of the exchange interactions in the temperature range from -10 to -8 K, suggesting the presence of strong interactions between the spin of the oxygen molecule and edge-state spin. A theoretical analysis effectively explains the interaction mechanism on the basis of the interaction between the electric dipole of the edge state and the quadrupole of the adsorbed oxygen molecule. This finding, which demonstrates an important role of exchange interactions between the graphitic π electrons and the spin of the adsorbed oxygen molecules, suggests that the adsorbed oxygen molecules are weakly bonded to the graphitic planes through charge transfer.

DOI: [10.1103/PhysRevB.76.035442](https://doi.org/10.1103/PhysRevB.76.035442)

PACS number(s): 73.63.-b, 73.22.-f, 75.30.Et, 81.05.Uw

I. INTRODUCTION

Nanosized materials have shown increasing relevance to materials science and cutting-edge device technologies for their unique and useful physical and chemical properties. In particular, nanosized carbon materials, such as carbon nanotubes and fullerenes, have been intensively investigated as nanoscience and/or nanotechnology subjects in recent years. Nanosized graphite (nanographite) is also included in the family of nanosized carbon materials. In contrast to carbon nanotubes and fullerenes (having closed π -electron systems), nanographite and nanographene (single-layer nanographite) are planar π -electron systems having an open-edge structure. Recently, nanographite and/or nanographene has been found to have a nonbonding π -electron state (edge state) topologically originating from the edge structure.¹⁻⁶ According to these studies, the edge state appears at around the Fermi level in the case of zigzag-shaped edges, and it results in anomalous features in the electronic and magnetic properties of nanographite and/or nanographene. Therefore, the electronic structure of nanographite and/or nanographene becomes entirely different from that of bulk graphite exhibiting diamagnetic properties. Interestingly, the presence of localized spins of edge-state spins induces strong spin magnetism, where even ferromagnetism has been predicted.⁷ In addition, the edge-state spins embedded in the conduction π electrons are expected to govern the electron transport in nanographite systems.³

Activated carbon fibers (ACFs) are interesting nanographite-based materials that can be used to investigate the anomalous electronic and magnetic features of nanographite.⁸⁻¹⁰ A single strand of ACF consists of a three-

dimensional (3D) disordered network of metallic nanographite domains; each of these domains is composed of a stack of three to four nanographene sheets with a mean in-plane size of $2-3$ nm.¹¹ Naturally, they have huge specific surface areas ($\sim 2000-3000$ m²/g) due to the presence of nanosized pores (nanopores) between the nanographite domains,^{12,13} which can accommodate a large volume of guest species through physisorption and chemisorption processes. Around the edges of the nanographene sheets, there are localized spins that originate from the nonbonding π -electron states of the edge origin.^{5,9} Our recent study has revealed that the adsorption of guest species, such as water,¹⁴ bromine,¹⁵ oxygen,¹⁶ and so on, into the nanopores affects the magnetic features of the edge-state spins. Interestingly, the mechanical effect of the physisorbed nonmagnetic guest species generates an on and off magnetic switching phenomenon. From the viewpoint of host-guest interactions, the adsorption of magnetic oxygen molecules into the nanopores is one of the most interesting subjects for understanding the role of the magnetic edge state in the nanographite.

In the present study, we investigate the magnetotransport of ACFs as a function of the adsorption of magnetic oxygen molecules in comparison with that of nonmagnetic guest species such as helium, nitrogen, and argon. A theoretical analysis of the experimental results is carried out for elucidating the interaction mechanism between the adsorbed oxygen molecules and the edge-state spins.

II. EXPERIMENT

The ACF samples used in the experiments were a commercially available product (FR-20, Kuraray Chemical Co.

Ltd.), which was derived from phenol resin precursors after activation at temperatures of 1073–1373 K in oxygen, water, carbon dioxide, or other oxidizing atmospheres.^{12,17} The FR-20 sample has a specific surface area of $\sim 2000 \text{ m}^2 \text{ g}^{-1}$.

All the dc electrical conductivity measurements were carried out for a single fiber along the fiber axis by means of a two-point probe method using an electrometer and/or high-resistance meter (Keithley Co. Ltd., 6517) in the temperature range from 2 to 300 K under a magnetic field up to 15 T. The sample was mounted on a sample holder in a variable temperature insert of a cryostat equipped with a 15 T superconducting magnet (Oxford Instruments Co. Ltd.). In order to reduce the leakage current in the high-resistance measurement, a triaxial cable was used as the guarding system for the sample current. The electrical contacts of a single ACF were made from gold electrodes using a carbon paste. The interval between the electrodes and the diameter of a single fiber were $\sim 0.05 \text{ mm}$ and $\sim 10 \mu\text{m}$, respectively, as confirmed by the optical microscope and scanning electron microscope. To observe the effects of molecular adsorption on the ACF, a specially designed sample chamber was fabricated. This sample chamber enables continuous heating, evacuation, and atmosphere control without exposing the sample to air after a single ACF is set onto the sample mount. The wires and thermometer inside this chamber were confirmed (in advance) to be heat resistant and nonvolatile at 473 K by temperature-programmed desorption. The insulating resins of the wires were made of PTFE (poly-tetra-flouro-ethylene) or polyimide, and a rhodium iron thermometer (Oxford Instruments Co. Ltd., PHZ002) was placed on the sample mount. The use of the specially designed sample chamber enabled the investigation of the detailed behavior of the effect of gas adsorption on conductivity and provided a new insight into the electron transport of ACFs, following earlier papers,^{8,18} in which special care has not been taken with regard to sample handling and measurements. After setting a single ACF onto the mount, the heat treatment was carried out in vacuum well below 1×10^{-6} Torr at 473 K for 30 h in order to remove the adsorbed molecules. Subsequently, the atmosphere was controlled after the introduction of guest gaseous species; then, the electrical conductivity measurements were carried out. For atmosphere control, the nonadsorbed sample was held in vacuum, and the samples with adsorbed molecules were obtained by turning a chamber valve to introduce guest molecules ($\sim 1 \text{ atm}$) at room temperature or at a temperature in between the room temperature and their boiling temperatures (for example, oxygen at around 100 K and nitrogen at 77 K).

The magnetic susceptibility and magnetization measurements were carried out using a superconducting quantum interference device magnetometer (MPMS-5, Quantum Design Co. Ltd.) in the temperature range from 2 to 380 K in a magnetic field up to 5.5 T. The samples for the susceptibility measurements were vacuum sealed at room temperature in glass tubes or sealed in an oxygen atmosphere in glass tubes at room temperature after heat treatment at 473 K for 48 h at a vacuum level of approximately 1×10^{-6} Torr. The amount of oxygen molecules adsorbed in ACFs in the low-temperature region below the boiling point was estimated from the volume of the oxygen gas introduced in the sample

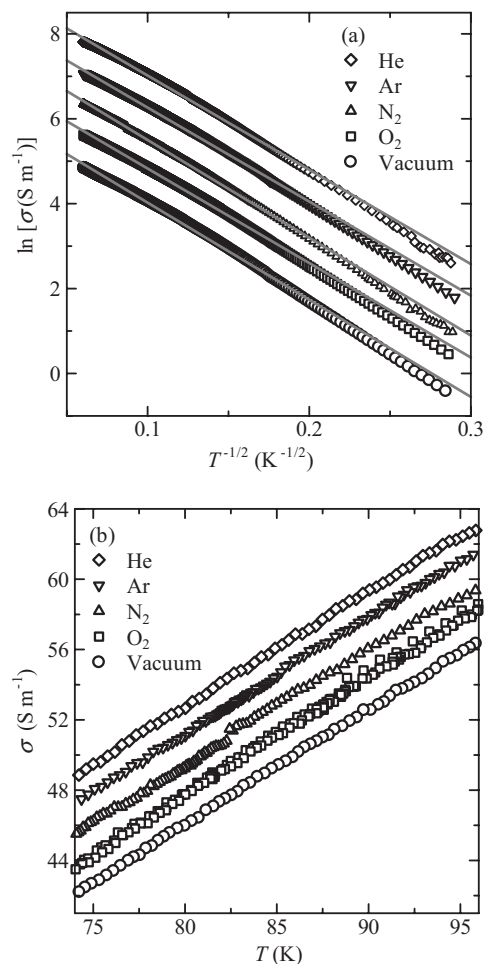


FIG. 1. (a) Temperature dependence of the conductivity σ ($\ln \sigma$ vs $T^{-1/2}$ plot) in the temperature range from 10 to 280 K. The solid line represents the fitting with the equation of the Coulomb-gap-type variable range hopping conduction. For clarity, the plots of the oxygen-adsorbed (\square), nitrogen-adsorbed (\triangle), argon-adsorbed (∇), and helium-adsorbed (\diamond) samples are shifted up by 0.75, 1.5, 2.25, and 3, respectively, with reference to the plot of the nonadsorbed sample (\circ). (b) The temperature dependence of conductivity in the temperature region from 74 to 96 K. For clarity, the data of the oxygen-adsorbed (\square), nitrogen-adsorbed (\triangle), argon-adsorbed (∇), and helium-adsorbed (\diamond) samples are shifted up by 1, 6.5, 6.5, and 7, respectively.

chamber at room temperature; this was confirmed by the change in the magnetization upon oxygen molecule uptake.

III. RESULTS

Figure 1(a) shows the conductivity vs temperature plots ($\ln \sigma$ vs $T^{-1/2}$) for the ACF samples in vacuum and in the atmospheres of the guest molecules (helium, argon, nitrogen, and oxygen). For all the samples in vacuum and gas atmosphere, the conductivity conforms to the Coulomb-gap-type variable range hopping formula^{19–21} expressed as

$$\sigma = \sigma_{\infty} \exp[-(T_0/T)^{1/2}], \quad (1)$$

where σ_{∞} is the conductivity at $T = \infty$; further, T_0 is given as

TABLE I. Values of T_0 and σ_∞ in the Coulomb-gap-type variable range hopping mechanism for the nonadsorbed sample and the samples adsorbed with oxygen, nitrogen, argon, and helium.

	Vacuum	Oxygen	Nitrogen	Argon	Helium
T_0 (K)	$(5.2 \pm 0.2) \times 10^2$	$(5.0 \pm 0.2) \times 10^2$	$(5.3 \pm 0.2) \times 10^2$	$(4.9 \pm 0.2) \times 10^2$	$(5.1 \pm 0.2) \times 10^2$
σ_∞ (S m ⁻¹)	$(5.5 \pm 0.2) \times 10^2$	$(5.5 \pm 0.2) \times 10^2$	$(5.5 \pm 0.2) \times 10^2$	$(5.1 \pm 0.2) \times 10^2$	$(5.3 \pm 0.2) \times 10^2$

$$T_0 = \frac{6e^2}{\pi k_B} \frac{1}{4\pi\epsilon_r\epsilon_0} \frac{1}{\xi}, \quad (2)$$

where ϵ_r , ϵ_0 , and ξ are the dielectric constant of the sample, permittivity of vacuum, and localization length, respectively. The conductivity behavior is in good agreement with that obtained in an earlier report,⁸ which suggests that the inter-nanographite-domain hopping process governs the electron transport in the Coulomb-gap-type variable range hopping mechanism. The values of σ_∞ and T_0 obtained from the fitting of the experimental results to Eqs. (1) and (2) are summarized in Table I. There are only small differences (-6% to $+2\%$) between the values obtained from the samples in vacuum and those in the atmospheres of the guest molecules. In addition, as shown in Fig. 1(b), there is no observable change in the conductivity values at the respective boiling temperatures of the adsorbed molecule species (90 K for oxygen, 77 K for nitrogen, and 87 K for argon), below which these adsorbed molecules condense in the nanopore space. This suggests that the electron transport mechanism is not seriously affected by the molecular adsorption at temperatures ranging from 10 to 300 K.

Figures 2 and 3 show the plots of magnetoresistance vs magnetic field at $T=2.19$ K in the magnetic field up to 15 T for the nonadsorbed and molecule-adsorbed ACF samples. The magnetoresistance MR is defined as

$$\text{MR} = \frac{R(H) - R(0)}{R(0)}, \quad (3)$$

where $R(H)$ is the resistance as a function of the magnetic field. In Fig. 2, a large positive magnetoresistance is observed, where its value is a concave function of the applied field. The value indeed goes up to $\sim 670\%$ at 2.19 K under a magnetic field of 15 T in the nonadsorbed sample and also in the presence of the nonmagnetic guest molecules (helium, nitrogen, and argon). The magnetoresistance is replotted in the double logarithmic scale in Fig. 2(b). The plots prove that the functional form of the plot of MR vs H cannot be represented by a quadratic function, unlike the case of typical semiconductors.²² The comparison of such plots of MR vs H reveals the presence of only a negligible difference in the behavior of the magnetoresistance between the nonadsorbed and nonmagnetic molecule-adsorbed samples, as shown in Fig. 2(b). The negligible effect of the nonmagnetic molecules on the magnetoresistance is also confirmed by the result of the nitrogen-adsorbed sample in which the nanopores are completely filled with nitrogen molecules after 1 atm of nitrogen is introduced at its boiling point, 77 K.¹¹ As shown in Fig. 3, in the presence of magnetic oxygen molecules, however, the positive magnetoresistance is reduced to $\sim 40\%$ of

that of the nonadsorbed sample when 1 atm of oxygen is introduced at room temperature. This finding proves that the magnetic moment of the adsorbed oxygen molecules is responsible for this change.

In Fig. 4, the temperature dependence of the magnetoresistance at 15 T is plotted in the low-temperature range of 2.2–4.0 K for the nonadsorbed and oxygen-adsorbed ACF

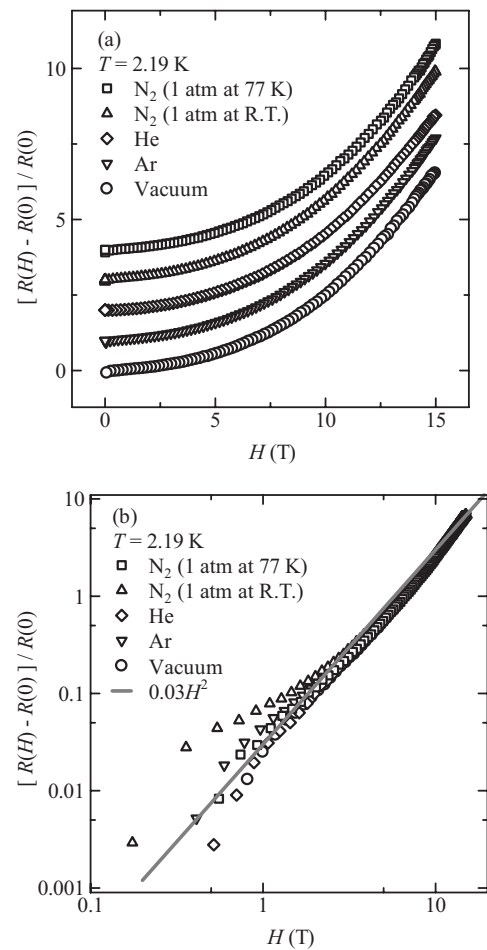


FIG. 2. (a) Magnetic field dependence of the magnetoresistance for the nonadsorbed (\circ) and nonmagnetic-molecule-adsorbed samples at 2.19 K. Further, 1 atm of nitrogen gas is adsorbed at 77 K and room temperature, while 1 atm of helium or argon is adsorbed at room temperature. For clarity, the plots of the argon-adsorbed (∇ , 1 atm at room temperature), helium-adsorbed (\diamond , 1 atm at room temperature), nitrogen-adsorbed (Δ , 1 atm at room temperature), and nitrogen-adsorbed (\square , 1 atm at 77 K) samples are shifted up by 1, 2, 3, and 4, respectively. (b) The double logarithmic plot of the magnetoresistance vs magnetic field. The solid line represents a quadratic function ($0.03H^2$).

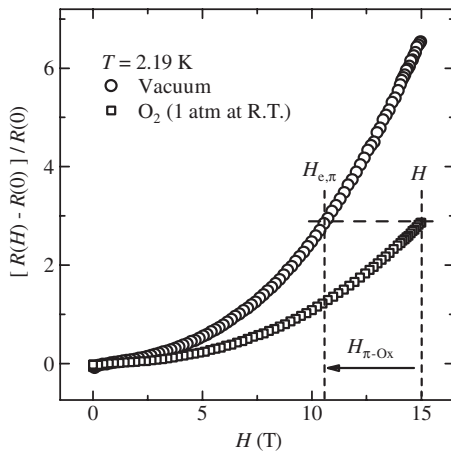


FIG. 3. Magnetic field dependence of the magnetoresistance for the nonadsorbed ACFs (\circ) and the oxygen-adsorbed ACFs (\square); 1 atm of oxygen molecules is adsorbed at room temperature for the latter case. $H_{e,\pi}$ and $H_{\pi-Ox}$ are the effective field acting on an edge-state spin and the internal field of the oxygen molecules acting on an edge-state spin, respectively. See text for details.

samples. The magnetoresistance of the nonadsorbed sample steeply increases up to 670% when the temperature is lowered to 2.19 K. The adsorption of the oxygen molecules considerably reduces the temperature dependence, where the effect of the oxygen molecules becomes stronger as the temperature decreases. Actually, the magnetoresistance decreases by 46% and 75% (at 3.60 K) and 56% and 80% (at 2.36 K) for the samples in which 1 atm of oxygen is adsorbed at room temperature and at 100 K, respectively. Figure 4 also shows that the increment in the magnetoresistance for the nonadsorbed sample is 4.3 when the temperature is lowered from 4 to 2 K, whereas this value is 1.6 and less than 1 for the oxygen-adsorbed samples in which 1 atm of oxygen is introduced at room temperature and at 100 K, respectively.

Figure 5 shows the magnetization curves at 2.0 K for the nonadsorbed and oxygen-molecule-adsorbed samples. The

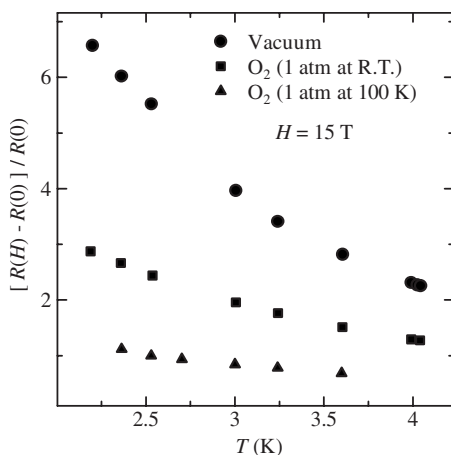


FIG. 4. Temperature dependence of the magnetoresistance at 15 T for the nonadsorbed sample (\bullet) and the samples into which 1 atm of oxygen molecules is adsorbed at room temperature (\blacksquare) and 100 K (\blacktriangle).

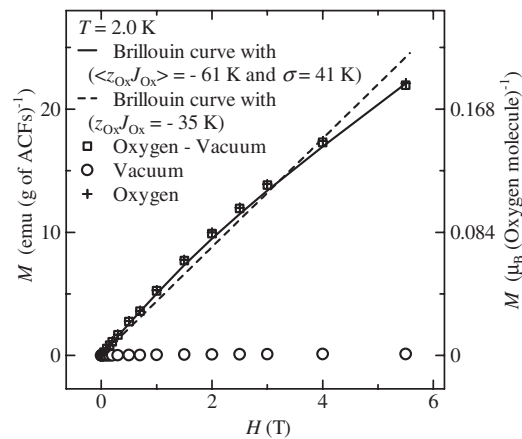


FIG. 5. Magnetization curves of the nonadsorbed sample (\circ), oxygen-adsorbed sample ($+$), and adsorbed oxygen molecules (\square) at 2.0 K. The amount of adsorbed oxygen molecules is 6.8×10^2 mg (g of ACFs) $^{-1}$. The solid curve is the fitting to the Brillouin curve ($S=1$), in which the distribution of the internal field values is considered. A Gaussian distribution is employed with a mean value of $\langle z_{Ox} J_{Ox} \rangle = -61$ K and standard deviation $\sigma = 41$ K, where the positive region of $z_{Ox} J_{Ox}$ is excluded. The dashed curve is the Brillouin curve ($S=1$) with a unique internal field value $z_{Ox} J_{Ox} = -35$ K. See text for the definitions of z_{Ox} , J_{Ox} , and σ .

magnetization of the oxygen-adsorbed sample is ~ 100 times larger than that of the nonadsorbed sample. The amount of adsorbed oxygen is estimated to be 6.8×10^2 mg (g of ACFs) $^{-1}$, which corresponds to ~ 200 oxygen molecules accommodated in a nanopore; here, the average volume of a nanopore (4.2 nm^3) is taken into account.¹² The magnetic susceptibility of the oxygen-adsorbed ACFs at 55 K is calculated to be 3.4×10^{-4} emu (g of oxygen) $^{-1}$, which is almost the same as that of solid oxygen at 54 K [3.19×10^{-4} emu (g of oxygen) $^{-1}$].^{23,24} This means that the magnetization in the oxygen-adsorbed sample is governed by the contribution of the spins ($S=1$) of the adsorbed oxygen molecules. Therefore, by subtracting the magnetization of the nonadsorbed sample from that of the oxygen-adsorbed sample, we estimate the magnetization of the adsorbed oxygen molecules, as shown in Fig. 5; here, we assume the additivity of the magnetization contributions of the ACFs and the adsorbed oxygen molecules because of the small contribution of the former. Here, the value of magnetization ($0.18 \mu_B$) at 5.5 T, which is the largest magnetic field investigated, is 1 order of magnitude smaller than the expected saturation magnetization ($= g_{Ox} \mu_B S = 2 \mu_B$ for $S=1$, where g_{Ox} is the g value of the oxygen molecule). This means that the spins of the oxygen molecules are strongly coupled to each other through antiferromagnetic interactions. This is consistent with the fact that the presence of antiferromagnetic couplings has been found not only in the solid oxygen phase²³ but also in the condensed state of oxygen molecules in the nanopores of ACFs.²⁵

Here, we estimate the strength of the internal field acting on the spin of an oxygen molecule. The effective field of the adsorbed oxygen molecule $H_{e,Ox}$ is given as

$$H_{e,Ox} = H + H_{Ox} + H_{Ox-\pi}, \quad (4)$$

where H_{Ox} and $H_{Ox-\pi}$ are the internal field of the oxygen molecules acting on the spin of the oxygen molecules and that of the edge-state spins acting on the spin of the oxygen molecules, respectively. The contribution of $H_{Ox-\pi}$ can be neglected because of the small number of edge-state spins existing in the nanographite domains (one to three spins per nanographite domain) in contrast to the large number of magnetic oxygen molecules in the nanopore (~ 200 per nanopore). The magnetization of the adsorbed-oxygen-molecule spins M_{Ox} is given as

$$M_{Ox} = N_{Ox} g_{Ox} \mu_B B_{S=1}(H_{e,Ox}) \approx N_{Ox} g_{Ox} \mu_B B_{S=1}(H + H_{Ox}), \quad (5)$$

if H_{Ox} has a unique value. Here, N_{Ox} , μ_B , and $B_{S=1}(H)$ are the number of adsorbed-oxygen-molecule spins per unit amount of ACFs, Bohr magneton, and Brillouin function for $S=1$, respectively. The mean-field treatment can relate M_{Ox} to the internal field H_{Ox} given as

$$H_{Ox} = \left[\frac{2}{N_{Ox} (g_{Ox} \mu_B)^2 z_{Ox} J_{Ox}} \right] M_{Ox}, \quad (6)$$

where z_{Ox} and J_{Ox} are the number of nearest-neighbor adsorbed oxygen molecules around each molecule and the exchange interaction parameter between the spins of the oxygen molecules, respectively. Here, the value of $z_{Ox} J_{Ox}$ is assumed to be the same for all the nearest-neighbor interactions. The fitting of magnetization to Eqs. (5) and (6) yields $z_{Ox} J_{Ox} = -35$ K as the exchange field of the oxygen molecules acting on the spin of an oxygen molecule. However, it should be noted that there is a deviation from the experimental result in the Brillouin curve fitting, as shown in Fig. 5. This is reasonably understood since the oxygen molecules adsorbed in the nanopores form a disordered structure in which the strengths of the exchange field vary randomly in space.¹⁶ Therefore, the distribution of the exchange field values should be introduced in the molecular field analysis. Indeed, a slightly convex magnetization curve in the experimental result demonstrates the distribution of the field strengths in which the magnetization of the oxygen molecules interacting through weaker interactions has a convex feature in the lower magnetic field range. On the basis of the necessity of the field distribution in the analysis, the following Gaussian distribution function is employed:

$$P(z_{Ox} J_{Ox}) = \frac{1}{\sqrt{2\pi}\sigma} \exp\left[-\frac{(z_{Ox} J_{Ox} - \langle z_{Ox} J_{Ox} \rangle)^2}{2\sigma^2}\right], \quad (7)$$

$$z_{Ox} J_{Ox} \leq 0,$$

where $\langle z_{Ox} J_{Ox} \rangle$ is the mean value and σ is the standard deviation, $\sqrt{\langle (z_{Ox} J_{Ox} - \langle z_{Ox} J_{Ox} \rangle)^2 \rangle}$. In the distribution function, the positive value region is excluded because the exchange interaction between the spins of the oxygen molecules is usually antiferromagnetic. By using Eq. (7), the magnetization can be expressed as

$$M_{Ox}(H, \langle z_{Ox} J_{Ox} \rangle, \sigma) = \int P(z_{Ox} J_{Ox}) M[H + H_{Ox}(z_{Ox} J_{Ox})] d(z_{Ox} J_{Ox}), \quad (8)$$

where $H_{Ox}(z_{Ox} J_{Ox})$ is a function of $z_{Ox} J_{Ox}$. The fitting of Eq. (8) effectively reproduces the experimentally observed magnetization curve with the mean value of $\langle z_{Ox} J_{Ox} \rangle = -61$ K and $\sigma = 41$ K, as shown in Fig. 5.

IV. DISCUSSION

A. Effect of adsorbed magnetic oxygen molecules on electron transport

As discussed in previous papers,^{8,18} the Coulomb-gap-type variable range hopping in the electron transport indicates the importance of the electron correlation effect on the inter-nanographite-domain electron hopping process. The insensitivity of conductivity to the adsorption of the guest gases proves that only a slight change takes place in the interdomain hopping process under the presence of guest molecules, including the magnetic oxygen molecule whose magnetic susceptibility is considerably small in the temperature range in which the conductivity is investigated. Comparing a previous study²⁶ on conductivity, the thermoelectric power and Raman spectra in relation to oxygen molecule adsorption reveal the manner in which the adsorbed oxygen molecules modify the electronic structure of the nanographite. The conductivity of the nonadsorbed sample is slightly increased with a change in the sign of the thermoelectric power from negative to positive upon oxygen molecule uptake. At the same time, the Raman experiment indicates a low frequency shift in the stretching mode of the oxygen molecules. These findings prove the presence of a slight charge transfer from the nanographite to the adsorbed oxygen molecules, even though its effect on interdomain hopping is small.

The important change in the electron hopping process is evident from the large positive magnetoresistance, which is seriously influenced by the adsorption of magnetic oxygen molecules. Further, this effect is enhanced as the temperature decreases. Therefore, a discussion should be devoted to the effect of molecular adsorption on the magnetoresistance. In general, a large positive magnetoresistance in the hopping process can be explained in terms of the spin-polarization effect^{27,28} and the wave-function shrinkage effect.^{28,29} In the former case, the electron in a domain is allowed to hop to the neighboring domain only if it has the spin state with a spin orientation opposite to that of the electron that has already been accommodated, as shown in Fig. 6. The application of a magnetic field, which forces all the spins to be oriented parallel to its direction, reduces the hopping rate, resulting in a large positive magnetoresistance (as observed). In the latter case, the wave-function shrinkage under the magnetic field reduces the wave-function overlap. In the present experiment, the former seems to be the major effect in comparison to the latter. The latter is usually applicable in doped semiconductors such as germanium, silicon, and their derivatives, where the decay length of the wave function of the impurity

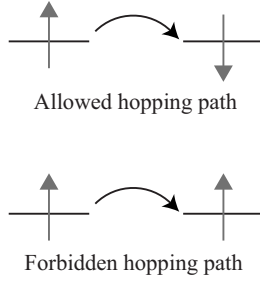


FIG. 6. Allowed and forbidden hopping paths depending on the spin orientation between the edge-state spins on the neighboring nanographite domains.

electron is usually greater than 10 nm and can be easily squeezed by the magnetic field.²⁹ However, the nonbonding π electrons on the edge site of the nanographite having a decay length of approximately 0.2–0.3 nm (Ref. 30) are hardly squeezed by the magnetic field.

From Fig. 4, it can be seen that the magnetoresistance increases with decreasing temperature. This result is qualitatively consistent with the proposed spin-polarization mechanism of the positive magnetoresistance. Indeed, as the temperature decreases, a decrease in the spin fluctuation leads to an increase in the forbidden hopping rate. Therefore, this leads to a larger positive magnetoresistance (as observed).

The important feature of the magnetoresistance is the large molecular adsorption effect, which appears when magnetic oxygen molecules are introduced as guest species, as shown in Figs. 3 and 4. For understanding the effects of oxygen molecule adsorption on the magnetoresistance, we focus our discussion on the internal magnetic field of the spins of the oxygen molecules because it can modify the spin orientations of the edge-state spins, resulting in a change in the magnetoresistance. More precisely, the antiferromagnetic internal field of the spin of the oxygen molecules acting on the edge-state spin competes with the external applied field and therefore the net effective magnetic field becomes smaller than the external applied field, resulting in a smaller magnetoresistance.

In the crystalline state of the oxygen molecules below the freezing point of 54.4 K, the spins of the oxygen molecules ($S=1$) are ordered antiferromagnetically through successive phase transitions from the γ phase to the β phase at 43.8 K and from the β phase to the α phase at 23.9 K. Here, the strengths of the antiferromagnetic interaction J are estimated as $J_\alpha \sim -30$ K, $J_\beta \sim -22$ K, and $J_\gamma \sim -14$ K.²³ The oxygen molecules accommodated in the nanopores form clusters with their disordered structures, as revealed in a previous study.²⁵ Therefore, the localized spins are randomly frozen in an antiferromagnetic spin-glass state at low temperatures. The deviation of the magnetization curve from the Brillouin function having an internal field with a unique value is indicative of the disordered spin structure with a wide distribution of the strengths of the exchange interaction, as discussed in the previous section. The estimated mean value of the exchange interaction, $\langle z_{\text{Ox}} J_{\text{Ox}} \rangle = -61$ K, is within a reasonable range when the strength of the exchange interactions in the crystalline state of the oxygen molecules is considered.

Here, we estimate the strength of the antiferromagnetic internal field of the oxygen molecules that acts on the π -electron spin of the edge state on the basis of the mean-field treatment for the magnetoresistance. The effective field $H_{e,\pi}$ to the π -electron spins is expressed as

$$H_{e,\pi} = H + H_{\pi\text{-Ox}} + H_\pi, \quad (9)$$

where $H_{\pi\text{-Ox}}$ and H_π are the internal field of the oxygen molecules acting on an edge-state spin and that of the edge-state spins acting on an edge-state spin, respectively. The internal field H_π is expressed by the magnetization of the edge-state spin M_π , while $H_{\pi\text{-Ox}}$ is given as Eq. (10) by considering the exchange interactions between the spin of the oxygen molecule and the edge-state spin:

$$H_{\pi\text{-Ox}} = \left[\frac{2}{N_{\text{Ox}} (g_{\text{Ox}} \mu_B)^2} \langle z_{\pi\text{-Ox}} J_{\pi\text{-Ox}} \rangle \right] M_{\text{Ox}}, \quad (10)$$

where $z_{\pi\text{-Ox}}$ and $J_{\pi\text{-Ox}}$ are the number of nearest-neighbor adsorbed oxygen molecules around one edge-state spin and the exchange interaction parameter between the spin of the oxygen molecule and the edge-state spin, respectively. Here, we take the average value as $\langle z_{\pi\text{-Ox}} J_{\pi\text{-Ox}} \rangle$ since $z_{\pi\text{-Ox}}$ and $J_{\pi\text{-Ox}}$ are randomly distributed due to the disordered structures of the oxygen molecule clusters. We can expect lesser interactions between the edge-state spins than that between the edge-state spin and the spin of the oxygen molecule, because the distance [~ 1 nm (Ref. 12)] between the edge-state spins on the adjacent domains is much larger than that between the edge-state spin and the spin of the oxygen molecule. Therefore, H_π can be neglected in this analysis. In addition, the magnetization of the edge-state spins M_π is much smaller than that of the spins of the adsorbed oxygen molecules M_{Ox} , as shown in Fig. 5.

According to a theoretical analysis,³¹ the magnetoresistance can be expressed in terms of a universal function with respect to temperature and the effective field acting on an edge-state spin as follows:

$$\frac{R(H)}{R(0)} \propto \cosh^2 \left(\frac{1}{2} \frac{g_\pi \bar{\mu}_B H_{e,\pi}}{k_B T} \right), \quad (11)$$

where g_π and $\bar{\mu}_B$ are the g value and effective Bohr magneton of the edge-state spin, respectively. We employ the effective Bohr magneton ($\bar{\mu}_B = 0.3 \mu_B$) since the edge state has a fractional magnetic moment according to theoretical calculations.² Equation (11) reveals that the functional form of the MR vs H curve in the nonadsorbed ACF sample holds well in the oxygen-adsorbed ACF sample when the applied field H is replaced with the effective field $H_{e,\pi}$. In other words, the magnetoresistance is uniquely dependent on the strength of the net effective field, regardless of the presence and/or absence of oxygen molecules in the nanopores. Based on this consideration, the difference in the applied magnetic field values between the nonadsorbed and oxygen-adsorbed samples at a given magnetoresistance value yields the internal field $H_{\pi\text{-Ox}}$ of the spins of the oxygen molecules, as shown in Fig. 3. According to the results shown in Fig. 3, the applied field dependence of the internal field is given as that shown in Fig. 7. The estimated internal field, which is pro-

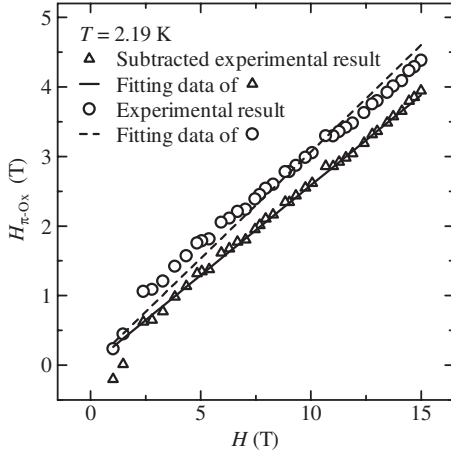


FIG. 7. Plot of the internal field $H_{\pi-Ox}$ of the spins of the oxygen molecule as a function of the applied field at 2.19 K. Circles and triangles represent the raw data and the plot corrected by vertically shifting the plot such that the extrapolation of the plot meets the origin at $H=0$. The solid and dashed lines represent $\langle z_{\pi-Ox} J_{\pi-Ox} \rangle = -8.1$ K and $\langle z_{\pi-Ox} J_{\pi-Ox} \rangle = -9.6$ K, respectively.

portional to the magnetization of the spins of the oxygen molecules, should be extrapolated to the origin when the applied field goes to zero, according to the behavior expected from Eqs. (9) and (10). However, the result shown in Fig. 7 exhibits a deviation from the expected behavior. The negligence of the internal field from the edge-state spins and the simplified model employed are considered to be responsible for this deviation. Therefore, a simple correction is made by vertically shifting the plot for the extrapolation to meet the expectation. The values of the exchange field parameter $\langle z_{\pi-Ox} J_{\pi-Ox} \rangle$ are estimated as -9.6 and ~ -8.1 K from the fittings at $T=2.19$ K without and with the correction, respectively, using the parameters $\langle z_{Ox} J_{Ox} \rangle = -61$ K and $\sigma = 41$ K (obtained in Sec. III). The results of the exchange field parameter for different temperatures are summarized in Table II.

B. Origin of strong magnetic interaction between the spin of the adsorbed oxygen molecule and the edge-state spin

The estimated strength of the internal field of the spins of the oxygen molecules acting on an edge-state spin is 2 orders of magnitude larger than that expected from the contribution of the magnetic dipole-dipole interaction, which is usually observed in the interaction between the physisorbed mag-

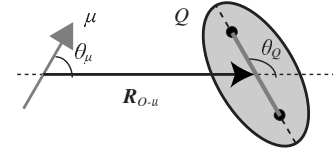


FIG. 8. The electric dipole-quadrupole interaction between the edge state and oxygen molecule. μ , Q , $R_{Q-\mu}$, θ_Q , and θ_{μ} are the electric dipole on the edge site of the nanographite, quadrupole moment of the oxygen molecule, distance vector from the center of the dipole μ to that of the quadrupole Q , the angle formed by the intersection of the oxygen molecular axis with $R_{Q-\mu}$, and the angle formed by μ with $R_{Q-\mu}$, respectively.

netic guest and the magnetic site of the host. Generally, oxygen molecules that are facing a graphene sheet can have the strength of the magnetic dipolar interaction in the temperature range from 0.01 to 0.05 K, where we assume that the mean distance between the graphene sheet and the oxygen molecule facing it ranges from 0.3 to 0.36 nm (according to density functional theory calculations).³²⁻³⁴ In addition, it should be noted that the superexchange mechanism, which is generally exhibited by molecular magnets, cannot operate here as the distance is too far for the superexchange interaction to occur. Therefore, the experimental finding, which demonstrates a strong exchange interaction between the graphitic π -electron spin and the adsorbed-oxygen-molecule spin, requires a new mechanism of electronic interaction. This is also supported by the Raman scattering, conductivity, and thermoelectric power measurements of the ACFs adsorbing the oxygen molecules,²⁶ as discussed in Sec. IV A. The mechanism of this strong interaction can be explained in terms of the interaction between the electric dipole at the edge site on nanographene and the electric quadrupole of the oxygen molecule, since it effectively reproduces the observed strength of the internal field. The detailed mechanism is given elsewhere.³¹ Here, we briefly discuss the mechanism for comparing the experimental results and the theoretical estimation. The scheme of the interaction between the electric dipole of the edge state on nanographene μ and the electric quadrupole of an adsorbed molecule Q is shown in Fig. 8. The edge state, which appears at the nanographene edge, has the largest population of edge carbon atoms bonded to foreign species. Therefore, electric dipoles are created at the graphene edge at which the edge state is present.

The exchange field parameter $\langle z_{\pi-Ox} J_{\pi-Ox} \rangle$ is estimated by a second-order perturbation with a perturbed Hamiltonian for the dipole-quadrupole interaction $\hat{H}_{Q-\mu}$:

TABLE II. Strengths of the exchange field parameter. See text for correction in the exchange field parameter.

T (K)	2.19	2.36	2.53	3.00	3.24	3.60	3.99
$\langle z_{\pi-Ox} J_{\pi-Ox} \rangle$ (K) (with correction)	-8.1	-7.9	-7.0	-6.5	-6.5	-5.9	-5.5
$\langle z_{\pi-Ox} J_{\pi-Ox} \rangle$ (K) (without correction)	-9.6	-9.6	-10	-9.3	-8.9	-8.5	-8.1

$$\hat{H}_{Q-\mu} = \frac{3Q\mu}{2R_{Q-\mu}^4} \cos \theta_\mu (3 \cos^2 \theta_Q - 1), \quad (12)$$

where $R_{Q-\mu}$, θ_μ , and θ_Q are the distance between the electric dipole μ and quadrupole Q , the angle formed by μ with the vector $R_{Q-\mu}$, and the angle formed by the intersection of the oxygen molecular axis with $R_{Q-\mu}$, respectively, as shown in Fig. 8. The vector $R_{Q-\mu}$ stretches from the center of μ to that of Q . The second-order perturbation process is mediated by the electron transfer between the edge state and the oxygen molecule; the latter is in the triplet state of ${}^3\Sigma_g(O_2)$. After taking the directional average for θ_Q , the second-order perturbation energy ΔE_2 can be expressed as

$$\Delta E_2 = \frac{1}{R_{Q-\mu}^8} \exp\left(\frac{-2R_{Q-\mu}}{a}\right) \frac{2z_{\pi-Ox}(3Q\mu)^2}{-E_{I,O} + E_{A,C} + \frac{e^2}{R_{Q-\mu}}}, \quad (13)$$

where $E_{I,O}$ and $E_{A,C}$ are the ionization energy of the oxygen molecule and the electron affinity of nanographite, respectively.

The factor $\exp(-2R_{Q-\mu}/a)$ accounts for the overlap of the wave functions between the edge state and the adsorbed oxygen molecule, where a is the decay length of the wavefunction overlap between the oxygen molecule and the edge state of the nanographite. The term $-e^2/R_{Q-\mu}$ in the denominator is the Coulomb interaction between the positively ionized oxygen molecule O_2^+ and the negatively charged nanographite domain. To evaluate ΔE_2 , the following parameters are adopted: $z_{\pi-Ox}=4$ (Ref. 35), $R_{Q-\mu}=0.44$ nm, $a=0.2$ nm (Refs. 30,36), $Q=-2.82 \times 10^{-25}$ esu cm² (Ref. 37), $\mu=2 \times 10^{-18}$ esu cm, $E_{I,O}=12.07$ eV (Ref. 38), and $E_{A,C}=4.6$ eV (Ref. 39). Then, ΔE_2 is calculated to be $\Delta E_2=-10$ K. This calculated value is in good semiquantitative agreement with the values $\langle z_{\pi-Ox} J_{\pi-Ox} \rangle \approx -10$ to -8 K obtained experimentally in Sec. IV A.

From the above calculation, we demonstrate that the dipole-quadrupole interaction is responsible for the microscopic origin of the antiferromagnetic exchange interaction between the edge-state spin and the adsorbed-oxygen-molecule spin.

V. CONCLUSION

Activated carbon fibers consist of a random 3D network of nanographite domains; each of these domains is composed of a stack of three to four nanographene sheets. We investigate the interdomain electron transport in relation to the magnetic field dependence and effects of molecular adsorption with argon, nitrogen, helium, and oxygen used as the guest molecules.

Nanopores created between nanographite domains lead to huge specific surface areas, and they can accommodate various guest molecules by the physisorption process. The electron transport is subjected to the Coulomb-gap-type variable range hopping mechanism with a negligible effect of molecular adsorption. The application of a magnetic field induces a large positive magnetoresistance at low temperatures. This indicates that the spin-polarization effect governs the interdomain electron transport in which the spins of the π -electrons originating from the edge state play an important role.

The adsorption of magnetic oxygen molecules considerably reduces the magnetoresistance in contrast to a small effect of the adsorption of nonmagnetic molecules on the magnetoresistance. This is explained in terms of the competition between the applied field and the antiferromagnetic internal field of the spins of the oxygen molecules acting on the π -electron spin. Further, it indicates that the exchange interaction has a major contribution to the internal field instead of the dipole-dipole interaction, which usually occurs between the physisorbed magnetic species and the magnetic site of the host system. The analysis of the experimental results suggests that the interaction of the electric dipole created at the graphene edge with the electric quadrupole of the adsorbed oxygen molecule is responsible for the large exchange interaction.

ACKNOWLEDGMENTS

The authors would like to express their gratitude to T. Kawakami and K. Yamaguchi for the fruitful discussions. This work was supported by a Grant-in-Aid for Scientific Research (No. 15105005) from the Japan Society for the Promotion of Science (JSPS).

¹S. E. Stein and R. L. Brown, J. Am. Chem. Soc. **109**, 3721 (1987).

²M. Fujita, K. Wakabayashi, K. Nakata, and K. Kusakabe, J. Phys. Soc. Jpn. **65**, 1920 (1996).

³K. Wakabayashi, M. Fujita, H. Ajiki, and M. Sigrist, Phys. Rev. B **59**, 8271 (1999).

⁴Y. Niimi, T. Matsui, H. Kambara, K. Tagami, M. Tsukada, and H. Fukuyama, Appl. Surf. Sci. **241**, 43 (2005).

⁵Y. Kobayashi, K. I. Fukui, T. Enoki, K. Kusakabe, and Y. Kaburagi, Phys. Rev. B **71**, 193406 (2005).

⁶Y. Kobayashi, K. I. Fukui, T. Enoki, and K. Kusakabe, Phys. Rev. B **73**, 125415 (2006).

⁷K. Kusakabe and M. Maruyama, Phys. Rev. B **67**, 092406

(2003).

⁸Y. Shibayama, H. Sato, T. Enoki, X. Bi, M. S. Dresselhaus, and M. Endo, J. Phys. Soc. Jpn. **69**, 754 (2000).

⁹Y. Shibayama, H. Sato, T. Enoki, and M. Endo, Phys. Rev. Lett. **84**, 1744 (2000).

¹⁰T. Enoki and Y. Kobayashi, J. Mater. Chem. **15**, 3999 (2005).

¹¹K. Kaneko, C. Ishii, M. Ruike, and H. Kuwabara, Carbon **30**, 1075 (1992).

¹²K. Oshida, K. Kogiso, K. Matsubayashi, K. Takeuchi, S. Kobori, M. Endo, M. S. Dresselhaus, and G. Dresselhaus, J. Mater. Res. **10**, 2507 (1995).

¹³M. El-Merraoui, H. Tamai, H. Yasuda, T. Kanata, J. Mondori, K. Nadai, and K. Kaneko, Carbon **36**, 1769 (1998).

- ¹⁴H. Sato, N. Kawatsu, T. Enoki, M. Endo, R. Kobori, S. Maruyama, and K. Kaneko, *Solid State Commun.* **125**, 641 (2003).
- ¹⁵K. Takai, H. Kumagai, H. Sato, and T. Enoki, *Phys. Rev. B* **73**, 035435 (2006).
- ¹⁶N. Kobayashi, T. Enoki, C. Ishii, K. Kaneko, and M. Endo, *J. Chem. Phys.* **109**, 1983 (1998).
- ¹⁷E. Tanaka, *Fuel Combust.(Nen-ryo nen-shou)* **54**, 241 (1987).
- ¹⁸A. W. P. Fung, M. S. Dresselhaus, and M. Endo, *Phys. Rev. B* **48**, 14953 (1993).
- ¹⁹N. F. Mott and E. A. Davis, *Electronic Processes in Non-crystalline Materials* (Oxford University Press, London, 1979).
- ²⁰A. L. Efros and B. I. Shklovskii, *J. Phys. C* **8**, L49 (1975).
- ²¹A. L. Efros, *J. Phys. C* **9**, 2021 (1976).
- ²²N. W. Ashcroft and N. D. Mermin, *Solid State Physics* (Thomson Learning, Stamford, 1976).
- ²³C. Uyeda, K. Sugiyama, and M. Date, *J. Phys. Soc. Jpn.* **54**, 1107 (1985).
- ²⁴David R. Lide, *CRC Handbook of Chemistry and Physics*, 81st ed., (CRC, Boca Raton, 2000).
- ²⁵N. Kobayashi, T. Enoki, Y. Murakami, H. Suematsu, and M. Endo, *Mol. Cryst. Liq. Cryst. Sci. Technol., Sect. A* **306**, 103 (1997).
- ²⁶G. U. Sumanasekera, S. Kishore, G. Chen, K. Takai, T. Enoki, and P. C. Eklund (private communication).
- ²⁷A. Kurobe and H. Kamimura, *J. Phys. Soc. Jpn.* **51**, 1904 (1982).
- ²⁸M. Pollak and B. I. Shklovskii, *Hopping Transport in Solids—Modern Problems in Condensed Matter Sciences* (North-Holland, New York, 1991).
- ²⁹B. I. Shklovskii and A. L. Efros, *Electronic Properties of Doped Semiconductors*, Springer Series in Solid-State Sciences Vol. 45 (Springer, Berlin, 1984).
- ³⁰F. A. Cotton, G. Wilinson, and P. L. Gaus, *Basic Inorganic Chemistry*, 3rd ed. (Wiley, New York, 1999).
- ³¹K. Sugihara, K. Takahara, K. Takai, and T. Enoki, *Phys. Rev. B* **75**, 205422 (2007).
- ³²D. C. Sorescu, K. D. Jordan, and P. Avouris, *J. Phys. Chem. B* **105**, 11227 (2001).
- ³³P. Giannozzi, R. Car, and G. Scoles, *J. Chem. Phys.* **118**, 1003 (2003).
- ³⁴Y. J. Xu and J. Q. Li, *Chem. Phys. Lett.* **400**, 406 (2004).
- ³⁵T. Enoki, *Hyoumen* **34**, 311 (1996).
- ³⁶M. Kotani, Y. Mizuno, K. Kayama, and E. Ishiguro, *J. Phys. Soc. Jpn.* **12**, 707 (1957).
- ³⁷A. D. Buckingham, *Chem. Br.* **1**, 54 (1965); T. A. Miller, *J. Chem. Phys.* **54**, 330 (1971).
- ³⁸S. G. Lias, J. E. Bartmess, J. F. Liebman, J. L. Holmes, R. D. Levin, and W. G. Mallard, *J. Phys. Chem. Ref. Data Suppl.* **17**, 1 (1988).
- ³⁹B. T. Kelly, *Physics of Graphite* (Applied Science, London, 1981).